Modelling sliding resistance of tolerably mobile subsea mudmats

X. Feng[1] and S. Gourvenec[1]

Published in *Géotechnique*, 66(6):490-499
doi: http://dx.doi.org/10.1680/jgeot.14-15.P.178

[1]Xiaowei FENG
Centre for Offshore Foundation Systems – M053
A node of the ARC Centre of Excellence in Geotechnical Science and Engineering
University of Western Australia
35 Stirling Highway, Crawley
Perth, WA 6009
Australia
Tel: +61 8 6488 2473
Fax: +61 8 6488 1044
Email: xiaowei.feng@uwa.edu.au

[1]Susan GOURVENEC
Centre for Offshore Foundation Systems
A node of the ARC Centre of Excellence in Geotechnical Science and Engineering
University of Western Australia
Tel: +61 8 6488 3995
Email: susan.gourvenec@uwa.edu.au

No. of words (without abstract and references):	4883
No. of tables:	3
No. of figures:	16

Modelling sliding resistance of tolerably mobile subsea mudmats

X. Feng[1] and S. Gourvenec[1]

ABSTRACT

Subsea infrastructure for deep-water oil and gas developments is often supported by mudmat foundations. Traditionally, subsea mudmats are designed to resist the loads imposed by pipeline thermal expansion and contraction while remaining stationary. As subsea facilities have grown, the required size and weight of the mudmats challenge the handling capacity of installation vessels and raises costs. Tolerable mobility of a subsea mudmat can significantly relieve the applied loads leading to reduced mudmat size and weight. In this paper, the cyclic shearing and reconsolidation response of fine-grained soil around a tolerably mobile mudmat is investigated through results of finite element analysis using a critical state soil model. The mudmat was subjected to a simulated lifetime of operation, with many cycles of undrained sliding with intervening consolidation between cycles. The sliding resistance was shown to rise exponentially with cycles and reach the drained limit, accompanied by significant strength gain in the subsoil because of the intervening consolidation between movements. The degree of reconsolidation between slides affects the number of cycles required to mobilize the drained limit. The hardening response for periodic shearing with intervening consolidation is shown to scale from the hardening response for continuous undrained shearing by an amount depending on the degree of intervening consolidation during pipeline operation. Expressions for the rate of hardening of sliding resistance of a tolerably mobile mudmat foundation are proposed in this paper to assist design practice.

[1] Centre for Offshore Foundation Systems, The University of Western Australia

1 **KEYWORDS**

2 clays; repeated loading; consolidation; footings/foundations; offshore engineering

INTRODUCTION

Subsea mudmats that support seabed infrastructure for deep-water oil and gas developments are subjected to cycles of operational loading as the attached pipelines undergo periodic thermal expansion and contraction during start up and shut down events during the life of field. Conventionally, subsea mudmats are designed to remain stationary by resisting all of the imposed operational loads. The emerging challenge is that as operational loading becomes more severe and seabeds become softer, the size and weight of mudmats derived from the traditional design methods (e.g. API, 2011; ISO, 2003) challenge the handling capabilities of many installation vessels and raise project costs. Provision of additional specialised vessels with heavy-lift capability, on top of a standard pipelaying vessel, affects the economic margins of a project.

Subsea geotechnical infrastructure may be designed to allow movement. Examples of cases in which mobility is currently accepted include controlled lateral buckling of on-bottom pipelines, trench development of steel catenary risers and the installation of drag-in plate anchors (Randolph et al., 2011). The concept of tolerably mobile subsea mudmats for supporting pipeline infrastructure allows a mudmat to slide on the seabed to accommodate pipeline expansion and contraction rather than resist the full expansion (or contraction) load. A tolerably mobile mudmat is also an alternative to the use of mechanical sliding mechanisms on the subsea structure to absorb expansions. Thus, operational load applied to the mat is relieved, allowing foundation size and weight reductions with potentially minimal operations during installation (Cathie et al., 2008, Cocjin et al., 2014, 2015a, Deeks et al., 2014).

A tolerably mobile subsea mudmat ideally slides repeatedly and reversibly in response to pipeline expansions and contractions. An analytical framework based on continuous planar shearing with concurrent drainage and consolidation was developed by Randolph et al. (2012) and applied to investigate the evolution of axial sliding resistance associated with pipeline

'walking'. Finite element analyses (Yan et al. 2014) extended the analytical framework to account for periodic shearing in which full primary consolidation occurs between pipe movements. Even though these works were focused on pipe-soil interaction, the theory can be used as rational guidance over the design of tolerably mobile mudmats. The potential of these mudmats to support subsea infrastructure has been demonstrated through centrifuge model testing (Cocjin et al., 2014, Stuyts et al. 2015). Methods to address aspects of design for tolerably mobile subsea mudmats have been suggested by Bretelle & Wallerand (2013), Deeks et al. (2014), Cocjin et al. (2015a,b), Zhou et al. (2015), although a systematic investigation of the sliding response of a tolerably mobile mudmat has not yet been presented.

This paper provides results from numerical analysis of a mobile mudmat on a normally consolidated fine grained seabed. Small-strain finite-element analysis and the critical state soil mechanics (CSSM) model, Modified Cam-Clay (MCC), are employed to couple the effects of soil shearing caused by foundation sliding, consolidation and soil strength gain. The evolution of horizontal sliding resistance within the lifetime of a mobile mudmat subjected to cyclic shearing and intervening reconsolidation is systematically investigated and the results are synthesized into expressions defining the rate of hardening to assist design practice. This work translates the study of Randolph et al. (2012) to mudmat foundations, and distils the outcomes into quantitative expressions to support design.

FINITE ELEMENT MODEL

All of the calculations were carried out using the Abaqus (v 6.10) program (Dassault Systèmes, 2010).

Model description

The boundary conditions considered in this study are illustrated schematically in Figure 1. A rigid, impermeable, surface rectangular mudmat with a breadth-to-length ratio, B/L = 0.5 was

considered. This aspect ratio is common for subsea mudmats and is often governed by the configuration of the opening on a pipe-laying vessel through which the mudmats are lowered to the seabed. The breadth of mat was taken as B = 5 m for all analyses (common in field applications), but results are presented as normalized quantities such that the actual dimension of the foundation is not relevant.

The interface between the underside of the mudmat and the subsoil was taken to be rough in shear with no detachment permitted (i.e. fully bonded). The mudmat remains in compression throughout the loading cycles such that no tendency for separation is observed. An example of a finite-element mesh used in this study is shown in Figure 2. The mesh boundaries extend a distance of 3B from the edges and 3B beneath the mat, with horizontally constrained nodes at the vertical sides, and fully constrained nodes at the base. Pore water flow was permitted across the top free surface of the mesh either side of the mudmat, but not across the mat, or the side or base boundaries of the mesh. Flow across the external vertical sides or base of the mesh was not expected as zones of excess pore water pressure generation were confined close to the mudmat and free surface, remote from the external boundaries.

The mat was modelled as a weightless, rigid body with a load reference point (LRP) located centrally at mudline level. However, a vertical load representing the self-weight of the structures was applied at the LRP to allow for generation of excess pore pressure and the following consolidation, as described later in the section of ‘Analysis programme’. Sliding was achieved by horizontal translation of the LRP with zero moment. The soil was represented by first-order fully integrated stress-pore fluid continuum elements.

Soil parameters

The critical state soil mechanics model in Abaqus, clay plasticity, was used with model parameters to represent Modified Cam Clay (MCC) (Roscoe & Burland 1968). The

implementation of MCC in Abaqus uses a Mises surface in the π-plane and associated flow by defining the flow stress ratio as unity. The numerical parameters used for the analyses are listed in Table 1. These properties are typical of the kaolin clay used for experimental research at The University of Western Australia (Stewart 1992). The soil was considered to be K_0-consolidated, with $K_0 = 1-\sin\varphi'_{tc}$, where φ'_{tc} is the friction angle for triaxial compression conditions.

A uniform surcharge, σ_{vo}, was applied at the upper soil surface (including across the weightless mudmat) to provide a nominal, non-zero value of shear strength at the mudline. The undrained shear strength profile was determined from the MCC input parameters using the expression proposed by Potts & Zdravkovic (1999).

$$\frac{s_u}{\sigma'_v} = g(\Theta)\cos\Theta\frac{1+2K_0}{3}\left(\frac{1+a^2}{2}\right)^{1-\frac{\kappa}{\lambda}} \quad (1)$$

where

$$g(\Theta) = \frac{\sin\varphi'_{cs}}{\cos\Theta + \left(1/\sqrt{3}\right)\sin\varphi'_{cs}\sin\Theta}$$

$$a = \frac{\sqrt{3}(1-K_0)}{g(-30^\circ)(1+2K_0)}$$

where Θ is the Lode's angle, taken as 0 to represent plane strain shear strength, and φ'_{cs} is the critical state angle of shearing resistance, g(-30º) is the value of g(Θ) for triaxial compression condition, i.e. Θ = -30º. The derived in situ soil properties are summarised in Table 2.

Analysis programme

Initially, the time-settlement response of the mudmat under self-weight loading was investigated and described by a continuous function to provide a reference for the degree of consolidation in subsequent analyses.

Secondly, a suite of analyses was carried out to define the sliding response over the undrained-drained transition. Continuous sliding of the mat foundation with concurrent drainage was modelled over a range of sliding velocities to investigate the interaction of slide velocity and cumulative time on the mudmat response. The analyses provide a backbone curve that defines benchmark values for fully undrained and fully drained sliding resistance, and the transition through dimensionless time.

Finally, analyses to mimic the operational mode of tolerably mobile mudmats were carried out. After geostatic conditions were achieved, a vertical load equivalent to the self-weight of the foundation and the supported structure was applied, representing touchdown on the seabed. The range of relative vertical load adopted is representative of field conditions. A period of excess pore pressure dissipation under the self-weight load was modelled to represent the delay between touchdown of the mudmat and pipeline operation. Subsequently, the mudmat was displaced horizontally to replicate forward sliding representing the response of the mudmat to pipeline expansion. The velocity of sliding was sufficiently fast to ensure undrained conditions in the subsoil, as would often be the case for the time periods relevant to pipeline “start-up”. The horizontal displacement was then maintained constant for an intervening period for dissipation of excess pore pressure, allowing full or partial consolidation, before reversing the slide to represent cooling and contraction of a pipeline during a “shut-down”. The procedure was repeated to represent the whole-life operation of the field. A schematic of the analysis procedure is presented in Figure 3.

RESULTS

Time-settlement histories post mudmat touchdown

The time-settlement responses of the mudmats under varying vertical load mobilisation of $v_p = V_p/V_{uu}$ were examined, where V_p represents the self-weight of the mudmat and the supported subsea structure and V_{uu} is the unconsolidated, undrained vertical bearing capacity.

$$V_{uu} = N_{cV} A s_{um} \quad (2)$$

where N_{cV} is the unconsolidated undrained vertical bearing capacity factor defined as a function of soil strength heterogeneity factor $\rho B/s_{um}$, ~ 10.69 for the soil considered in Table 2 (Feng et al, 2014). Only the time-dependent component of settlement was investigated, that is, the instantaneous settlement on touchdown was deducted from the total settlement. Time was represented by the dimensionless time factor

$$T_v = \frac{c_{v0}(t - t_1)}{B^2} \quad (3)$$

where $(t-t_1)$ is the time period since mudmat touchdown, and c_{v0} is the in situ coefficient of consolidation of the soil at the level of mudmat invert.

$$c_{v0} = \frac{1 + e_0}{\lambda} \frac{\sigma_{vo}}{k\gamma_w} \quad (4)$$

where e_0 is the in situ void ratio.

The degree of consolidation due to self-weight during the time lag between installation and pipeline operation was defined in terms of the normalised time-settlement response of the mudmat (Figure 4). The normalised responses are independent of the magnitude of v_p, reflecting the results by Feng & Gourvenec (2015), and can be approximated by a hyperbolic function

$$U_v = \frac{w}{w_f} = \frac{1}{1+(T_v/T_{v,50})^{-m_1}} \quad (5)$$

where $T_{v,50}$ is the dimensionless time factor for 50% of the consolidation settlement to occur following mudmat installation, and m_1 is an exponent. $T_{v,50}$ = 0.023 and m_1 = 1.16 gave the best fit of the finite-element results.

Undrained – drained continuum for continuous shearing

The effect of time and slide velocity on the sliding resistance of a subsea mudmat is explored, as analysed by Randolph et al. (2012) for the case of continuous planar shearing. The variation of horizontal sliding resistance with time is represented for different normalised velocities, vh_s/c_{v0}, where v is the velocity of mudmat sliding, h_s is the thickness of the shear band, here defined as the thickness of the layer of elements beneath the mat (≈ 1%B). The thin layer of elements under the foundation was selected so that the sliding resistance could be captured more accurately. If too thick, the sliding resistance would be significantly over-estimated because of shearing in a layer of elements of finite thickness rather than across an infinitesimal thickness interface. If too thin, the required initial time increment for stabilisation of the consolidation analyses (Vermeer & Verruijt, 1981) would become very short. This would require an extremely fast loading rate to achieve undrained condition in the soil and lead to unwanted oscillation in the model. Normalisation of the slide velocity by the thickness of the first layer of the elements was adopted after the concept proposed by Randolph et al. (2012) in their analytical analysis. For the current FE model, it is impossible to capture the 'real' shear band. An alternative here is to choose the thickness of the first layer of elements underneath the mudmat where the shearing occurred. Therefore, the so-called 'shear band' does not have a physical meaning. The normalised velocity of vh_s/c_{v0} is only a scale. It does not matter which dimension is chosen to normalise the velocity, since that the mobilised resistance is only determined by the velocity of slide.

The equivalent coefficient of sliding friction, $\mu = H/W'$ is shown in Figure 5 for a range of normalised sliding velocities for the case of $v_p = V_p/V_{uu} = 0.3$ with full primary consolidation following touchdown of the mudmat ($U_v = 1$). The dimensionless time factor is defined as

$$T_h = \frac{c_{v0}(t - t_2)}{B^2} \quad (6)$$

where $(t-t_2)$ is the elapsed time since the start of the sliding movement.

Separate mobilisation responses for each normalised velocity are intercepted by a common backbone curve. The undrained-drained backbone response provides benchmark values for fully undrained and fully drained sliding resistance, with the latter achieved at a time factor of $T_h \sim 1.6$. The normalised velocities $vh_s/c_{v0} = 10^3$ and 10^{-3} lead to responses that show no hardening over the displacement considered, being fully undrained and fully drained respectively.

The fully undrained sliding resistance following self-weight consolidation after touchdown, H_{cu} can be predicted using the power function proposed by Feng & Gourvenec (2015)

$$H_{cu} = U_v^{\,g}\left(H_{cu,max} - H_{uu}^*\right) + H_{uu}^* \quad (7)$$

where g is an exponent, ~ 0.705 for the mat geometry under consideration, H_{uu}^* is the unconsolidated, undrained horizontal resistance accounting for the vertical load mobilisation, v_p and it can be determined from the failure envelope for combined vertical and horizontal loading considering self-weight consolidation (Feng & Gourvenec, 2015). $H_{cu,max}$ is the maximum consolidated undrained horizontal resistance corresponding to full primary self-weight consolidation.

$$H_{cu,max} = \left(1 + RN_{cV} f_\sigma f_{su} v_p\right) H_{uu} \quad (8)$$

where R is the normally consolidated undrained strength ratio, s_u/σ'_v, N_{cV} is the unconsolidated undrained vertical bearing capacity factor, f_σ is a scaling parameter accounting

for the distribution of stress in the zone of soil affected by the operative vertical load, f_{su} is a scaling parameter to account for interaction of the zone of non-uniform distribution of the increased shear strength and soil involved in the sliding failure mechanism, v_p is the vertical load mobilisation due to mudmat self-weight, and H_{uu} is the unconsolidated undrained horizontal resistance. For a rectangular surface mudmat on a normally consolidated deposit, the proposed value of $f_\sigma f_{su}$ is 0.919 (Feng & Gourvenec 2015). The scaling parameter, $f_\sigma f_{su}$, has been shown to be valid to predict gains in foundation capacity for a range of practical soil properties, being applicable to normally consolidated clay conditions with soil properties other than those considered in this study, as shown in Table 1 (Feng & Gourvenec 2015), as well as in over-consolidated conditions (Gourvenec et al. 2014). The equivalent coefficient of sliding friction, $\mu = H/W'$ predicted during undrained sliding is 0.292 (Figure 5), comparable with the defined normally consolidated strength ratio of 0.286 for the soil.

The sliding resistance equals the integral of the mobilised shear stress over the foundation bearing area. For full drained shearing, the resistance

$$H_d = \sum_{i=1}^{j} \tau_{zx,i} A_i = \mu \sum_{i=1}^{j} \sigma'_z A_i = \mu W' \tag{9}$$

where j is the number of elements across the soil-foundation interface, A_i is the contact area of the i^{th} element and W' is the total normal force applied to the soil-foundation interface, $W' = V_p + \sigma_{vo}A$.

The stress states are shown in Figure 6 for a soil element at the level of the mudmat invert. At failure,

$$\begin{aligned} p'_f &= \sigma'_{xf} = \sigma'_{yf} = \sigma'_{zf} \\ q_f &= \sqrt{3}\tau_{zxf} \end{aligned} \tag{10}$$

The coefficient of friction for drained sliding

$$\mu = \frac{\tau_{zxf}}{\sigma'_{zf}} = \frac{q_f}{\sqrt{3}p'_f} = \frac{M}{\sqrt{3}} \tag{11}$$

The coefficient of friction obtained from the finite element analysis was approximately 0.555, over-predicting the theoretical value of 0.532 by 5% for the soil parameters given in Table 1. Equation (11) indicates that the coefficient of friction for fully drained sliding is dependent only on one of the MCC parameters, M, not the selected surcharge.

The backbone response represents the rate of hardening for undrained continuous shearing without intervening periods of rest, and is a function of the magnitude of the operative vertical load and the degree of self-weight consolidation between mudmat touchdown and pipeline operation. Figure 7 shows backbone curves for v_p = 0.3 and 0.5, and for varying degrees of consolidation post touchdown, U_v. The backbone response initially falls on individual curves at the undrained limit (Equation (7)), and gradually converges to the corresponding drained limit (Equation (11)) as time increases. The backbone curves in Figure 7 can be estimated by

$$\frac{H}{W'} = \frac{H_d}{W'} - \left(\frac{H_d}{W'} - \frac{H_{cu}}{W'}\right) 0.5^{\left(T_h/T_{h,50}\right)^{m_2}} \quad (12)$$

where $T_{h,50}$ is the time at which the frictional resistance is midway between the undrained and drained limits. $T_{h,50}$ = 0.02 and m_2 = 0.65 provide good fit to the backbone curves.

Periodic undrained sliding with intervening full primary consolidation

In this section, periodic undrained sliding with intervening full primary consolidation is considered for a selected vertical load mobilisation, taken as v_p of 0.3. The effect of the vertical load mobilisation and degree of intervening consolidation are discussed in the next section and the analysis procedure is generalised.

The periodic sliding events of the mudmat were carried out at a normalised velocity of vh_s/c_{v0} = 10^3 over a distance of 0.2B, ensuring a fully undrained condition was maintained during sliding. The intervening period of consolidation between each forward and reverse slide was sufficient to ensure complete dissipation of excess pore pressure. Figure 8 shows the

coefficient of sliding friction, μ = H/W', with normalised lateral displacement, u/B, under periodic undrained sliding with intervening full primary consolidation. The coefficient of sliding friction evolves from the undrained value, equivalent to the in situ undrained strength ratio R, and reaches the drained limit, given by Equation (11), within 15 episodes.

Figure 9 shows the cycle-by-cycle e-lnσ'_v path for a representative soil element beneath the centroid of the mudmat for full primary self-weight consolidation post touchdown, U_v = 1, and full primary intervening consolidation between slide events, U_i = 1, where U_i is defined by the time-settlement responses of the mudmat during the intervening periods of reconsolidation. During the initial forward slide of the mudmat (B→C in Figure 9), the effective vertical stress in the soil reduces as the stress path moves to the critical state line, CSL. The effective vertical stress then recovers to the initial self-weight value during the intervening reconsolidation (C→D), with associated pore pressure dissipation and void ratio reduction. The subsequent slides and intervening periods of reconsolidation result in successive generation and dissipation of excess pore pressure caused by sliding. The process repeats over the lifetime of the mudmat until the soil beneath the mat undergoes sufficient cycles of shearing, pore pressure generation and reconsolidation to reach a final critical void ratio (F), thereby eliminating any tendency for contraction and further excess pore pressure generation.

The rise in lateral sliding resistance resulting from periodic sliding events and intervening consolidation can be captured by an analytical framework (Figure 10a) of a form introduced in White and Hodder (2010) and extended in White et al. (2015), based on the gain in operative undrained strength that depends on the reduction in the void ratio, e, by Equation (13), which is a geometric sum of the gain in each cycle.

$$\frac{\ln s_u - \ln s_{ui}}{\ln s_{uf} - \ln s_{ui}} = \frac{\Delta e}{\Delta e_f} = \frac{\kappa'}{\lambda}\sum_{i=1}^{n}\left(1-\frac{\kappa'}{\lambda}\right)^{n-1} \quad (13)$$

where n represents the current number of slides completed and is equal to 2N, with N being the current number of episodes comprising two sliding and two reconsolidation events, which is equivalent to the number of operating cycles, i.e. start-up/shut-down cycles. κ' is the recompression index with respect to effective vertical stress σ'_v rather than the mean stress p'.

$$\kappa' = \frac{\Delta}{(\lambda-\kappa)\ln\left(\frac{3}{1+2K_0}\right)+\Delta}\kappa \tag{14}$$

where Δ is the change in void ratio between the CSL and the K_0 normally consolidated line (K_0-NCL) at a single effective stress level.

$$\Delta = e_N - e_{cs} - \ln\left[\left(\frac{3(1-K_0)}{M(1+2K_0)}\right)^2 + 1\right] \tag{15}$$

where e_N is the void ratio at p' = 1 kPa on the virgin compression line, NCL. The unload-reload gradient κ′ in e-lnσ'_v is approximately 0.033 based on the parameters listed in Table 1. The reduction in void ratio during each reconsolidation event depends on the unload-reload gradient κ′, while the final reduction depends on the steepness of the CSL, λ. The hardening process is therefore also independent of the selected surcharge. The results of the increase in the sliding resistance derived from the FE analysis show good agreement with the analytical solution yielded by Equation (13), where the basal sliding mechanism allows s_u, s_{ui} and s_{uf}, to be taken as being in the same proportions as H, H_{cu} and H_d (Figure 10b). Alternatively, an exponential relationship proposed by Yan et al. (2014) might be employed for predicting the resistance mobilised during the n^{th} slide

$$\frac{H-H_{cu}}{H_d-H_{cu}} = 1-0.5^{(n-1)/n_{50}} \tag{16}$$

where n_{50} is the number of cycles of movement and consolidation required to achieve 50% of the full hardening process for the frictional resistance, depending on the ratio of κ′/λ, given by Equation (17) as suggested by Yan et al. (2014).

$$n_{50} = \frac{0.9}{\kappa'/\lambda} \quad (17)$$

Figure 11 shows the reduction of the void ratio for the representative soil element beneath the centroid of the mudmat as shown in Figure 9, due to periodic undrained sliding with intervening full primary reconsolidation for the case of 30% completion of the self-weight consolidation post touchdown, i.e. U_v = 0.3, (A→B'). The only difference is the reduction in the void ratio during reconsolidation (C′→B) following the first slide (B′→C′), where the residual excess pore pressure due to mudmat touchdown and the newly induced excess pore pressure from undrained shearing have dissipated, with the effective vertical stress recovering to B. The e-ln(σ'_v) path for the following cycle of shearing and reconsolidation generally follows that as shown in Figure 9, for full primary consolidation following touchdown.

In contrast to undrained continuous shearing, the rate of hardening for sliding resistance for periodic shearing with intervening full primary consolidation is independent of the degree of the primary consolidation after touchdown, U_v, after the first cycle of foundation movement, and reached the drained limit after a cumulative time of T_h ~ 5 since the start of pipeline operation. All these cases show a much stiffer response compared with undrained continuous sliding (Figure 12). The evolution of the horizontal resistance for periodic shearing with intervening full primary consolidation (U_i = 1) can be predicted using Equation (12) but with different values of $T_{h,50}$ and m_2. $T_{h,50}$ = 0.7 and m_2 = 0.9 were found to give the best fit for this case.

The increase in the undrained shear strength along the centreline below the mudmat is shown in Figure 13. The initial soil strength profile was proportional to depth according to Equation (1), with a value of s_{um} = 1.431 kPa. After full primary consolidation under the operative vertical load, this mudline strength increased by 60 %, to 2.285 kPa. A simple estimation of the rise in the strength at mudline level, considering the soil element as indicated in Figure 9,

would be $e^{(e_1-e_{cs})/\lambda} \sim 1.9$ due to the periodic shearing and reconsolidation with e_1 being the intercept (~ 2.273) on e-ln(σ_v) at σ_v'= 1 kPa. The zone of strength gain extended approximately 0.3B beneath the mudmat, which is consistent with experimental observations from model tests of mobile foundations (Cocjin et al., 2015a).

Periodic undrained sliding with intervening partial consolidation

The generation and dissipation of excess pore pressure is concurrent for undrained continuous shearing if only partial consolidation has been achieved under the self-weight load ($U_v < 1$), whereas no residual excess pore pressure exists in the subsoil at the start of each individual slide for the case of undrained periodic sliding with intervening full primary consolidation ($U_i = 1$). In the field, the time lag between slide events of a mobile mudmat will be determined by the operation schedule of the attached pipelines. Table 3 summarises various intervening periods of reconsolidation for a mobile mudmat associated with different schedules of pipeline start-up and shut-down, with a constant degree of consolidation between mudmat touchdown and the start of pipeline operation ($U_v = 0.5$). The rate of hardening for sliding resistance for the example cases is plotted in Figure 14 along with the hardening responses for undrained continuous shearing, and for periodic shearing with full intervening primary consolidation. Figure 14 shows that the hardening responses for all the periodic shearing and reconsolidation cases are bracketed by that for undrained continuous shearing and periodic shearing with intervening full primary consolidation.

For the hypothetical cases considered, a reconsolidation period of t_{op} = 3 months (0.25 years, $T_{op} = t_{op}c_{v0}/B^2 \sim 2.23 \times 10^{-3}$) and t_{op} = 1.5 years ($T_{op} \sim 1.34 \times 10^{-2}$) immediately after the forward slide (i.e. pipeline start up) were respectively prescribed for Case-1 and Case-2, representing different periods for pipeline operation. The subsequent waiting period between the backward slide and the next forward slide (i.e. pipeline shut-down period), t_{sd}, was adopted as 1 day for both cases ($T_{sd} = t_{sd}c_{v0}/B^2 \sim 2.48 \times 10^{-5}$) to reflect field conditions. In

Case-3, the period for pipeline operation was identical with Case-2, but a 7-day period (T_{sd} ~ 1.73×10^{-4}) was prescribed for pipeline shut-down. The hardening response of Case-1 initially falls outside the backbone response for undrained continuous shearing before converging with the backbone curve with time. The hardening process in Case-2 and Case-3 overlap, indicating the independence of the hardening response from the relatively short shut-down period, t_{sd}. The curves for the hardening process for all of the five cases offset gradually towards that for the case of periodic shearing with full primary reconsolidation between slides with increasing intervening period of rest following the forward slide, t_{op}.

To predict the hardening process, Equation (12) is again adopted with m_2 maintained constant as 0.9 since all the curves are approximately parallel. The only variable for each case is the required time for achieving the midway of the corresponding undrained and drained limits of the horizontal resistance, $T_{h,50}$. The estimated values of $T_{h,50}$ for periodic shearing are presented in Figure 15 as a quadratic polynomial function of the equivalent time factor for the intervening consolidation period following the forward slide, t_{op}.

$$T_{h,50} = 7.5505T_{op}^{\ 2} + 3.1136T_{op} + 0.02 \quad (18)$$

t_{op} represents the meaningful consolidation, which in practice takes place in operation with negligible consolidation during the limited duration of shut downs.

Equations (12) and (18) are independent of the vertical load mobilisation v_p due to selected relative self-weight, and the degree of consolidation U_v following mudmat touchdown. Predictions of the hardening process for horizontal resistance for v_p = 0.3 and 0.5, and U_v = 0.3 derived from FE analyses are shown in Figure 16a and b compared with predictions from Equations (12) and (18).

Sensitivity of the gain in sliding resistance due to intervening partial consolidation on the selected surcharge was also examined. The FE results for a different surcharge of σ_{vo} = 16 kPa

in comparison with the base case value σ_{vo} = 5 kPa are well predicted by the Equations (12) and (18), indicating that the gain in sliding resistance due to intervening partial consolidation is insensitive of the surcharge (Figure 16c).

The procedure set out above enables prediction of the evolution of gain in horizontal resistance of a tolerably mobile mudmat under periodic sliding and intervening consolidation by scaling the hardening response for continuous undrained shearing by an amount depending on the degree of intervening consolidation between sliding events. The equations presented in this paper are relevant for the case of uniform periods of reconsolidation (of any degree) between each sliding event. The method can be modified to non-uniform periods of reconsolidation between sliding events by adopting a cycle-by-cycle approach using the analytical solution (Figure 10a), similar to that described by White et al. (2015) for prediction of pipeline walking.

Summary of procedure

Sliding resistance of a tolerably mobile mudmat under periodic shearing and reconsolidation resting on a normally consolidated soil can be predicted with the following procedure.

(a) Assess the unconsolidated undrained uniaxial capacity V_{uu}, and vertical load mobilisation, $v_p = V_p/V_{uu}$, for a given mudmat geometry, self-weight and in situ soil shear strength profile.

(b) Calculate the time factor T_v (Equation (3)) for a given time delay between mudmat touchdown and start-up of pipeline operation, based on the in situ coefficient of consolidation c_{v0} (Equation (4)). Determine the degree of consolidation U_v using the time factor T_v (Equation (5)).

(c) Evaluate the fully undrained horizontal resistance H_{cu} using Equations (7) and (8), and the fully drained horizontal resistance H_d through Equations (9) and (11).

(d) For a given intervening period of reconsolidation following the forward slide, t_{op}, estimate $T_{h,50}$ (for the hardening process to achieve midway between H_{cu} and H_d through Equation (18).

(e) Predict the hardening process giving the evolution of horizontal resistance using Equation (12).

CONCLUSIONS

The sliding resistance of a tolerably mobile subsea mudmat under periodic shearing and reconsolidation was investigated by finite element analyses. The gain in sliding resistance, or the 'hardening response', under periodic sliding with intervening consolidation has been shown to be bounded by the hardening response under undrained continuous shearing with concurrent consolidation, and periodic shearing with full primary consolidation between cycles. The hardening response for periodic shearing with intervening partial consolidation has been shown to be predicted by scaling the hardening response for undrained continuous sliding by an amount depending on the intervening period of reconsolidation during pipeline operation. The number of cycles of shearing and reconsolidation to reach the drained limit is governed by the ratio of κ'/λ and the degree of consolidation permitted between sliding events. Expressions and an analysis procedure are provided for predicting the hardening response of horizontal sliding resistance for tolerably mobile subsea mudmats on soft clay. The procedure has been proven general and applicable to MCC parameters and overburden stress other than those selected in this study.

ACKNOWLEDGEMENT

This work forms part of the activities of the Centre for Offshore Foundation Systems (COFS), established in 1997 under the Australian Research Council's Special Research Centres Program, and supported as a node of the Australian Research Council's Centre of

Excellence for Geotechnical Science and Engineering, and through the Fugro Chair in Geotechnics, the Lloyd's Register Foundation Chair and Centre of Excellence in Offshore Foundations and the Shell EMI Chair in Offshore Engineering. The first author is supported by the Lloyd's Register Foundation and ARC grant DP140100684. Lloyd's Register Foundation helps to protect life and property by supporting engineering-related education, public engagement and the application of research. The second author is supported through ARC grant CE110001009. The work presented in this paper is supported through ARC grant DP140100684. This support is gratefully acknowledged.

NOTATION

A	bearing area of mudmat
B	mudmat breadth
c_{v0}	in situ coefficient of consolidation
e_0	initial void ratio
e_{cs}	void ratio at p' = 1 kPa on CSL
f_σ	stress factor
f_{su}	shear strength factor
h_s	thickness of shear band
H_{cu}	consolidated undrained horizontal resistance
$H_{cu,max}$	maximum consolidated undrained horizontal resistance corresponding to fully primary consolidation following touchdown
H_{uu}	unconsolidated undrained horizontal resistance
H^*_{uu}	unconsolidated undrained horizontal resistance accounting for $v_p = V_p/V_{uu}$
k	soil permeability
K_0	coefficient of earth pressure at rest
L	mudmat length
n	current number of slides completed
N	current number of episodes comprising two sliding and two reconsolidation events, which is equivalent to the number of operating cycles, i.e. start-up/shut-down cycles
N_{cV}	unconsolidated undrained vertical bearing capacity factor
p'	mean effective stress
q_f	shear stress in the deviatoric plane at failure condition
R	normally consolidated undrained shear strength ratio, $R = s_u/\sigma'_v$
s_{ui}	in situ undrained shear strength
s_{uf}	undrained shear strength at critical state
s_{um}	undrained strength at mudline level
t	time
t_1	time at mudmat touchdown
t_2	time at the start of pipeline operation
T_v	time factor for the elapsed time since touchdown
$T_{v,50}$	time factor corresponding to 50% consolidation settlement since touchdown
T_h	time factor for the elapsed time since the start of pipeline operation
$T_{h,50}$	time factor at which the frictional resistance is midway between the undrained and drained limits
U_i	degree of intervening consolidation
U_v	degree of consolidation following touchdown
v	velocity of mudmat sliding

v_p	vertical load mobilisation, $v_p = V_p/V_{uu}$
V_p	vertical self-weight load
V_{uu}	unconsolidated, undrained vertical capacity
w	consolidation settlement following touchdown
w_f	consolidation settlement corresponding to full primary consolidation following touchdown
W'	submerged unit weight of mudmat
γ'	effective unit weight of soil
γ_w	unit weight of pore water
Θ	Lode's angle
κ	recompression index in e-lnp'
κ'	recompression index in e-lnσ_v'
λ	virgin compression index
μ	coefficient of sliding friction
ν'	Poisson's ratio
ρ	undrained shear strength gradient
σ'_v	vertical effective stress
σ'_{zf}	normal stress in z direction at failure
τ_{zxf}	shear stress in the xoz plane at failure
σ_{vo}	surcharge
φ'_{cs}	critical state angle of shearing resistance
φ'_{tc}	friction angle for triaxial compression

REFERENCES

API (2011) RP 2GEO Geotechnical and Foundation Design Considerations - 1st Edition. Washington, American Petroleum Institute.

Bretelle, S. & Wallerand, R. (2013). Fondations superficielles glissantespour l'offshore profond – methodologie de dimensionnement. In *Proc. of the 18th Int. Conf. on Soil Mechanics and Geotech. Eng. (ICSMGE)*, Paris (eds P. Delage, J. Descrues, R. Frank, A. Peuch and F. Schlosser), pp. 2331-2334.

Cathie, D., Morgan, N. & Jaeck, C. (2008) Design of sliding foundations for subsea structures In *BGA International Conference on Foundations*, Dundee, Scotland (eds M. J. Brown), pp. 24-27.

Cocjin, M., Gourvenec, S., White, D. & Randolph, M. F. (2014) Tolerably mobile subsea foundations: Observations of performance. Géotechnique 64(11):809-895, http://dx.doi.org/10.1680/geot.14.P.098.

Cocjin, M., Gourvenec, S., White, D. & Randolph, M. (2015a) Effects of drainage on the

response of a sliding subsea foundation. In *the 3rd Int. Sym. on Frontiers in Offshore Geotechnics (ISFOG 2015)*, Oslo, Norway (eds M. Vaughan), pp.777-782.

Cocjin, M., Gourvenec, S., White, D. & Randolph, M. F. (2015b) An effective stress framework for the degradation and recovery of surficial soil strength. submitted to journal.

Dassault Systèmes (2010). *Abaqus analysis users' manual*. Providence, RI, USA: Simulia Corp.

Deeks, A., Zhou, H., Krisdani, H., Bransby, F. & Waston, P. (2014) Design of direct on-seabed sliding foundations In *Proc. of the 33rd Int Conf. on Ocean, Offshore and Arctic Eng. (OMAE 2014)*, San Francisco, USA.

Feng, X., Randolph, M. F., Gourvenec, S. & Wallerand, R. (2014). Design approach for rectangular mudmats under fully three-dimensional loading. Géotechnique 64(1), 51–63, http://dx.doi.org/10.1680/geot.13.P.051.

Feng, X. & Gourvenec, S. (2015) Consolidated undrained load-carrying capacities of mudmats under combined loading in six degrees-of-freedom. Géotechnique, 65(7): 563-575. http://dx.doi.org/10.1680/geot./14-P-090.

Gourvenec, S., Vulpe, C. & Murthy, T. (2014). A method for predicting the consolidated undrained bearing capacity of shallow foundation. Géotechnique 64, No. 3, 215–225, http://dx.doi.org/10.1680/geot.13.P.101.

ISO (2003) ISO19901-4: Petroleum and natural gas industries specific requirements for Offshore Structures - Part 4: Geotechnical and foundation design considerations - 1st Edition. Geneva, International Standards Organisation.

Potts, D. M. & Zdravkovic, L. (1999) Finite element analysis in geotechnical engineering-Theory. Thomas Telford, London, UK.

Randolph, M. F., Gaudin, C., Gourvenec, S. M., White, D. J., Boylan, N. & Cassidy, M. J. (2011) Recent advances in offshore geotechnics for deep water oil and gas developments. Ocean Engineering 38(7):818-834.

Randolph, M. F., White, D. J. & Yan, Y. (2012) Modelling the axial soil resistance on deep-water pipelines. Géotechnique 62(9):837-846, http://dx.doi.org/10.1680/geot.12.OG.010.

Roscoe, K. H. & Burland, J. B. (1968) On the generalized stress-strain behaviour of wet clay. In Engineering Plasticity. (eds J., Heymen, and F. Leckie) Cambridge University Press, Cambridge, pp. 535-609.

Stewart, D. P. (1992) Lateral loading of piled bridge abutments due to embankment construction. PhD thesis, The University of Western Australia, Australia.

Stuyts, B., Wallerand, R. & Brown, B. (2015) A framework for design of sliding mudmat foundations. In *the 3rd Int. Sym. on Frontiers in Offshore Geotechnics (ISFOG 2015)*, Oslo, Norway (eds M. Vaughan), pp. 807-812.

Vermeer, P. A. & Verruijt, A. (1981). An accuracy condition for consolidation by finite elements. *Int. J. Numer. Anal. Methods Geomech.* 5, No. 1, 1–14.

White, D. J. & Hodder, M. (2010). A simple model for the effect on soil strength of episodes of remoulding and reconsolidation. Can. Geotech. J. 47, No. 7, 821–826, http://dx.doi.org/10.1139/T09-137.

White, D.J., Westgate, A., Ballard, J-C, de Brier, C. & Bransby, M.F. (2015) Best practice geotechnical characterization and pipe-soil interaction analysis for HPHT pipeline design. *Proc. Offshore Technology Conference*, Houston, OTC-26026-MS.

Yan, Y., White, D. J. & Randolph, M. F. (2014) Cyclic consolidation and axial friction for seabed pipelines. Géotechnique Letters 4:165-169, http://dx.doi.org/10.1680/geolett.14.00032.

Zhou, H., Krisdani, H., Maujean, R. & Deeks, A. D. (2015) System investigation of direct on-seabed sliding foundations. In *the 3rd Int. Sym. on Frontiers in Offshore Geotechnics (ISFOG 2015)*, Oslo, Norway (eds M. Vaughan), pp.825-830.

Table 1 Soil parameters for numerical studies

Parameter input for FE analysis	Values
Index and engineering parameters	
Saturated bulk unit weight, γ_{sat} : kN/m^3	16.0
Permeability of soil, k: m/s	1×10^{-9}
Unit weight of water, γ_w : kN/m^3	10.0
Porous elastic parameters	
Recompression index, κ	0.044
Poisson's ratio, ν'	0.3
Tensile limit	0
Clay plasticity parameters	
Virgin compression index, λ	0.205
Stress ratio at critical state, M = q/p' (friction angle in triaxial compression, φ'_{tc})	0.92 (23.5°)
Wet yield surface size, β	1.0
Flow stress ratio, K	1.0
Intercept on critical state line (CSL), e_{cs} (at p' = 1)	2.14

Table 2 In situ soil properties

Mudline strength, s_{um}: kPa	1.431
Strength gradient, ρ: kPa/m	1.717
Consolidation coefficient (in situ), c_{v0}: m^2/s	7.16×10^{-9}

Table 3 Matrix of prescribed operating conditions for mudmats

Case Number	Degree of primary consolidation under self-weight, U_v	Intervening periods of rest	
		Following forward slide (start-up), t_{op}	Following backward slide (shut-down), t_{sd}
1	0.5	0.25 years	1 day
2		1.5 years	1 day
3		1.5 years	7 days
4		5 years	7 days
5		10 years	7 days

Figure Captions

1

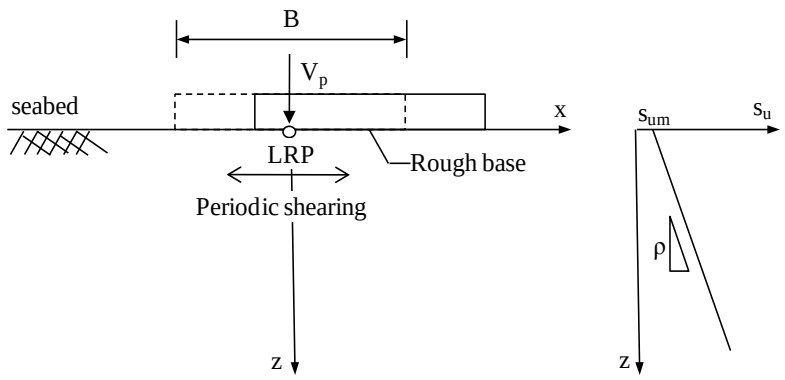

2

3 Figure 1 Schematic of a tolerably mobile mudmat on normally consolidated soil

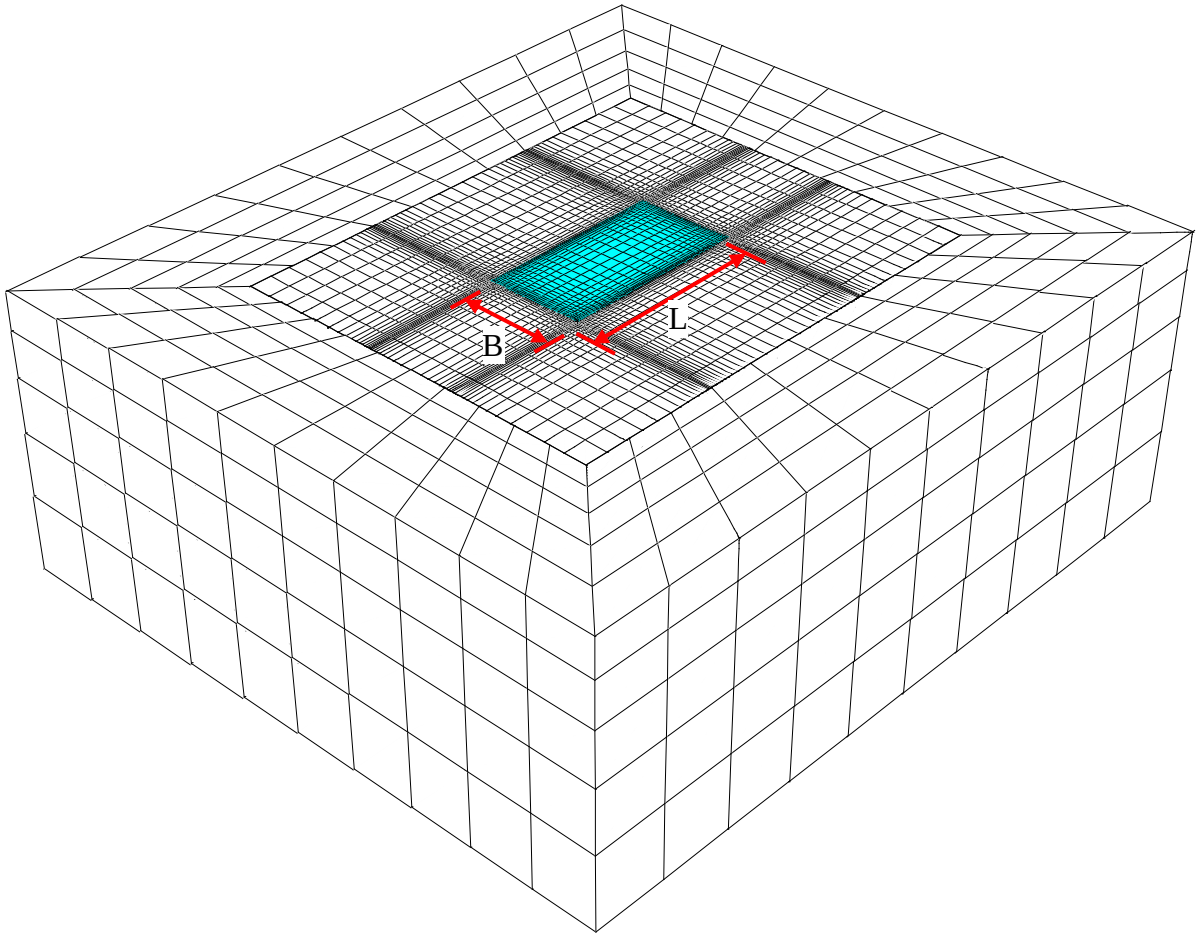

4

5 a) Isotropic view

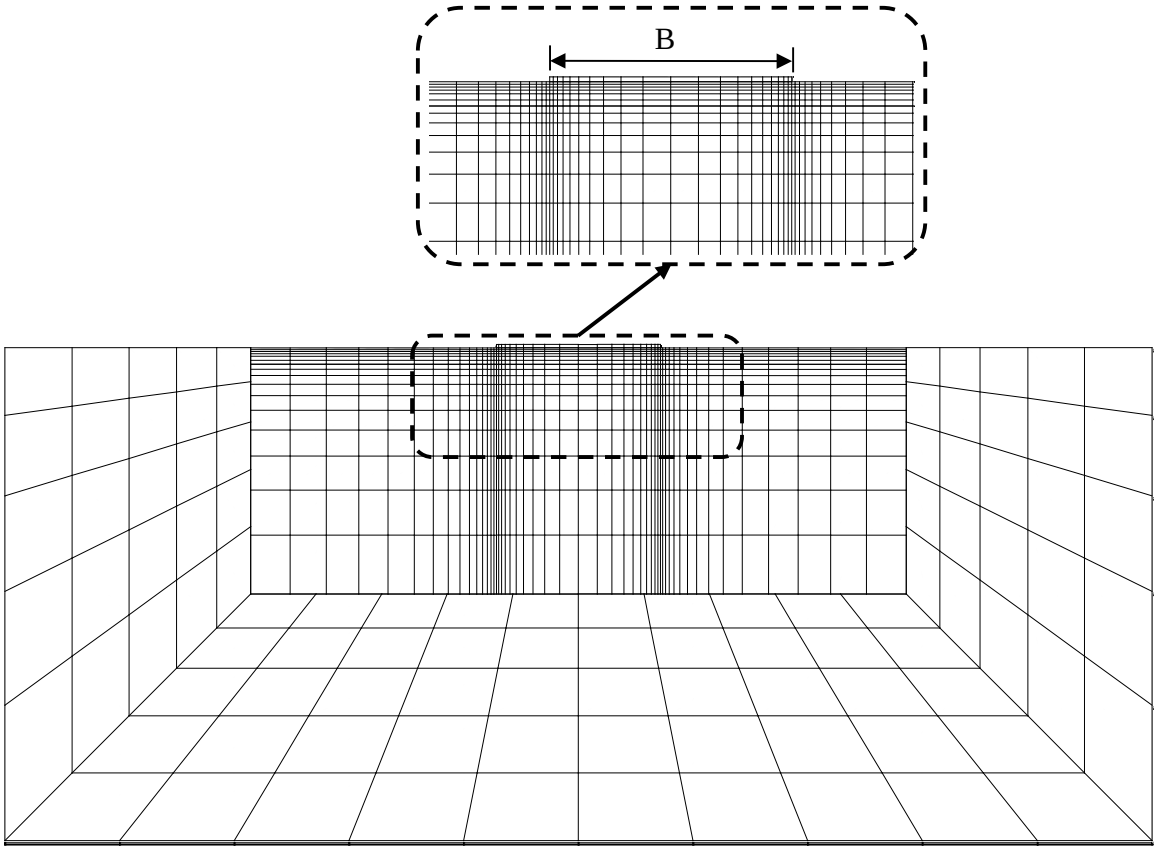

b) Elevation view through mid-point central plane

Figure 2 FE mesh for tolerably mobile mudmat

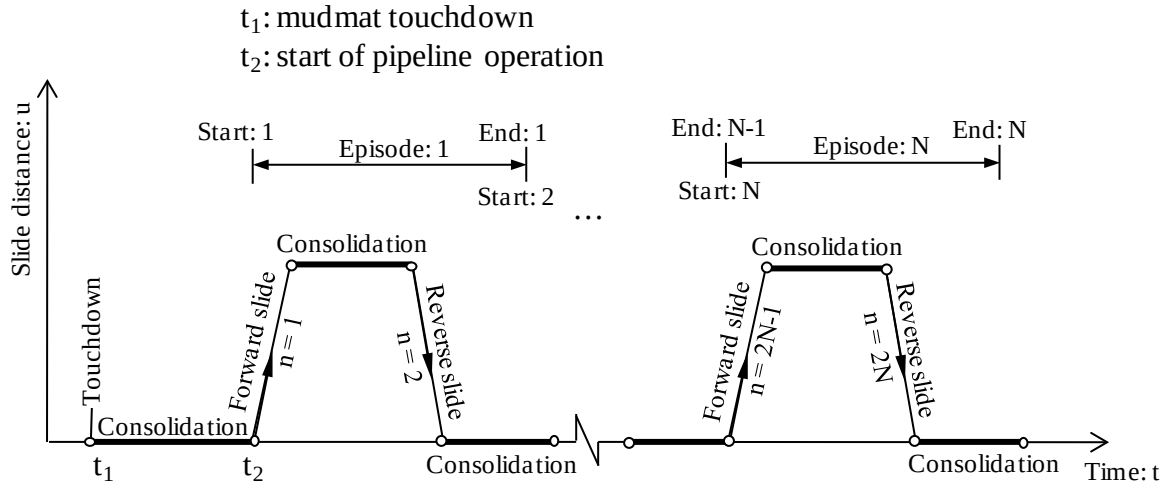

Figure 3 Schematic of the whole life response of a mobile mudmat

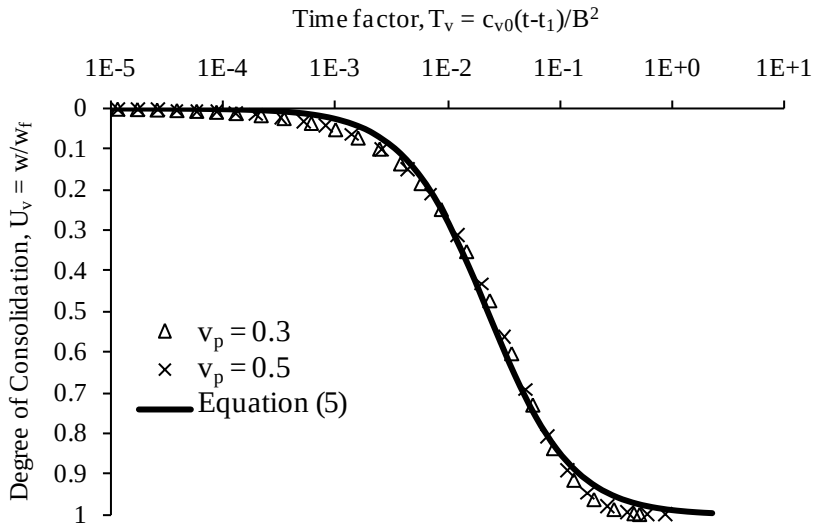

1

2 Figure 4 Normalised time–settlement response of mudmat under varying vertical load

3 mobilisation

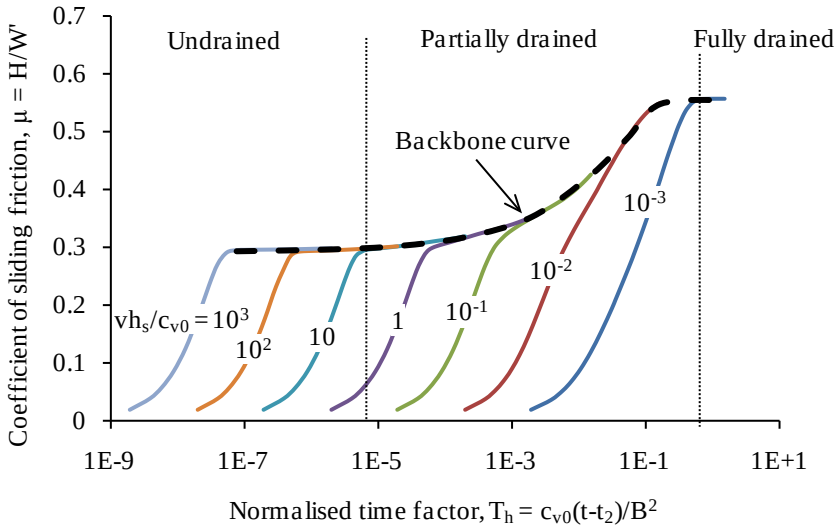

4

5 Figure 5 Monotonic sliding resistance at differing normalised velocities ($U_v = 1$)

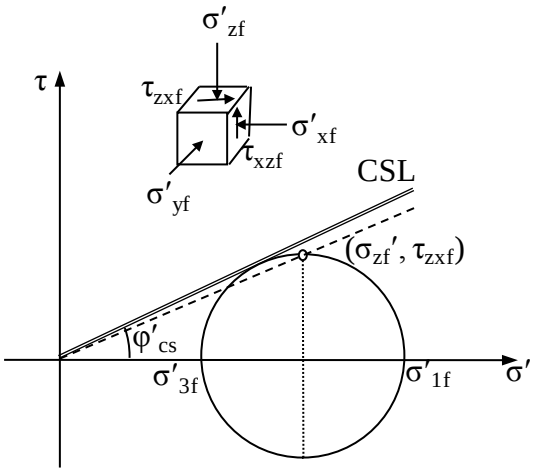

Figure 6 Stress states at failure for a representative soil element at mudmat invert

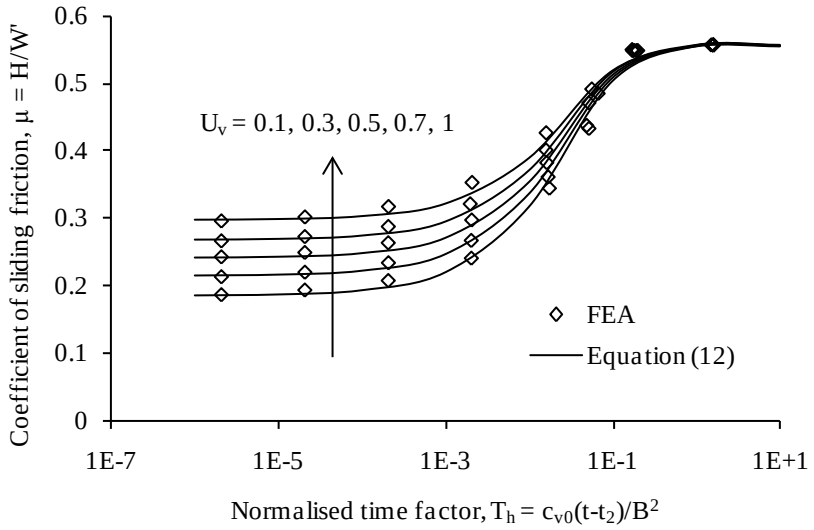

a) $v_p = 0.3$

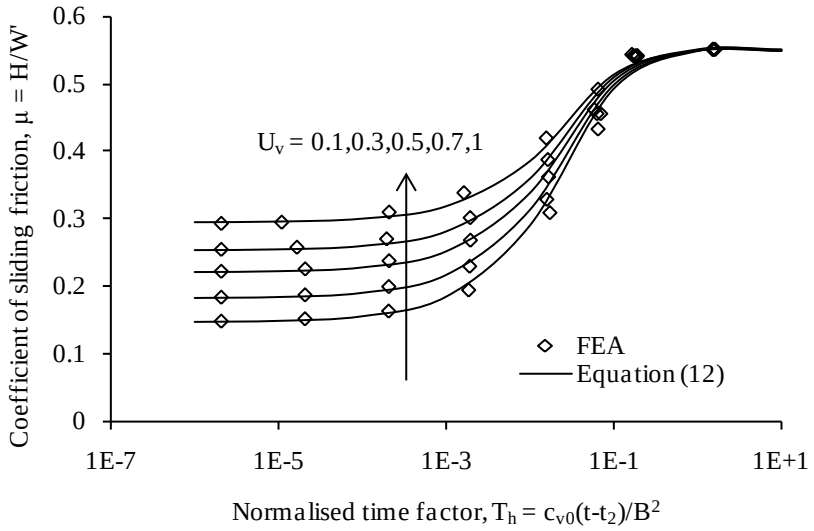

1

2 b) $v_p = 0.5$

3 Figure 7 Backbone response for undrained continuous sliding for varying operative vertical

4 load and degree of primary consolidation

5

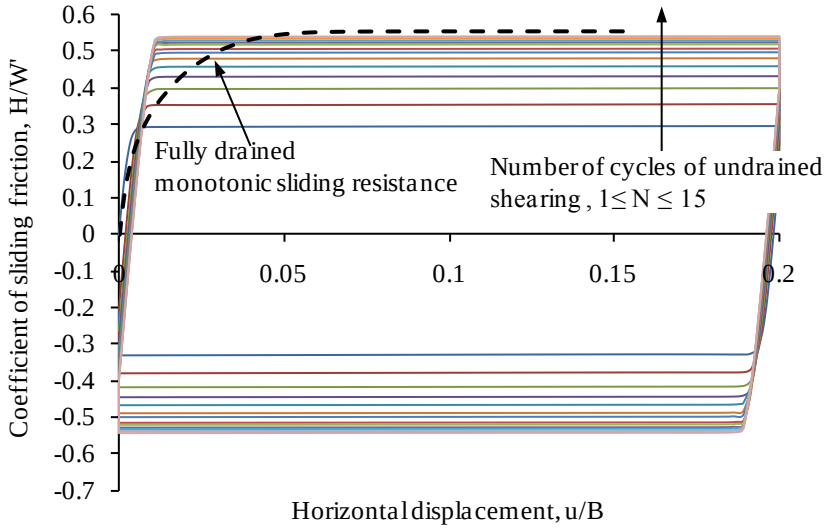

6

7 Figure 8 Evolution of coefficient of frictional sliding (U_v =1; U_i =1)

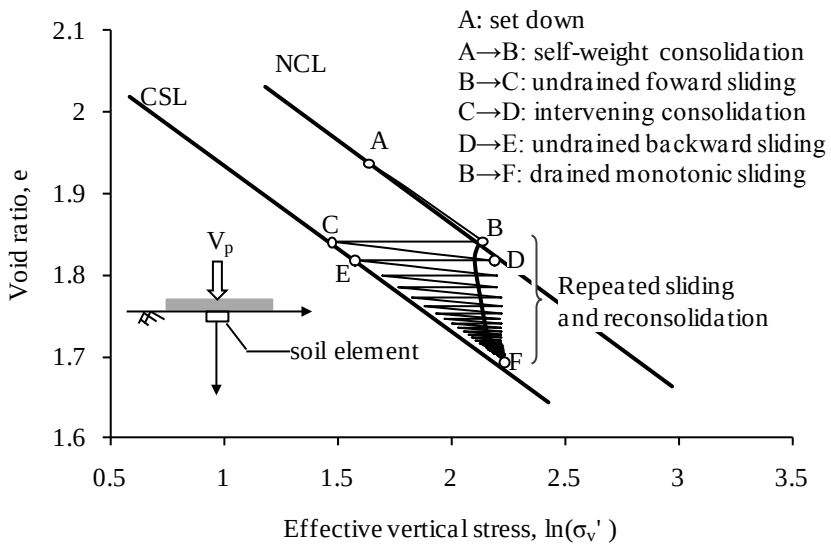

1

2 Figure 9 Stress-volume path of a representative soil element beneath mudmat (U_v = 1; U_i = 1)

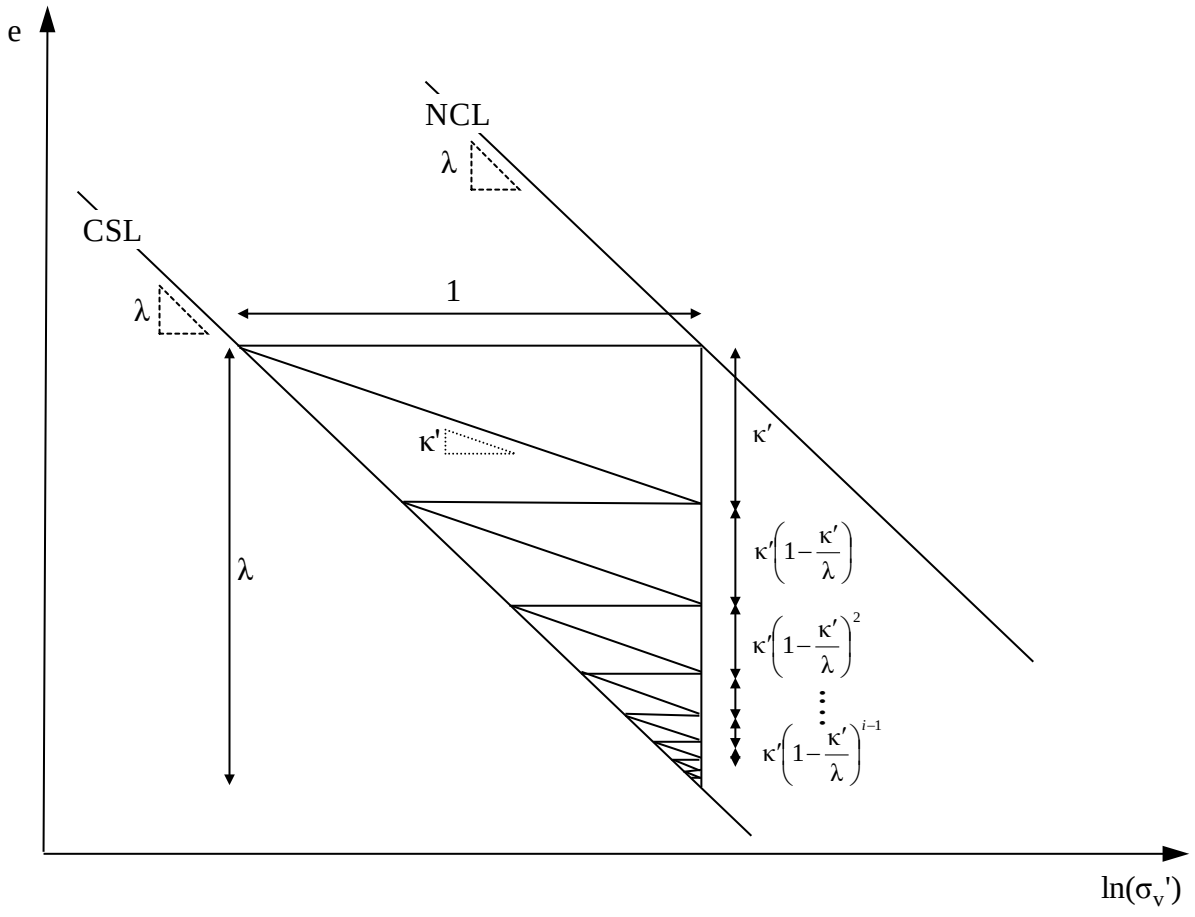

3

4 a) Analytical model

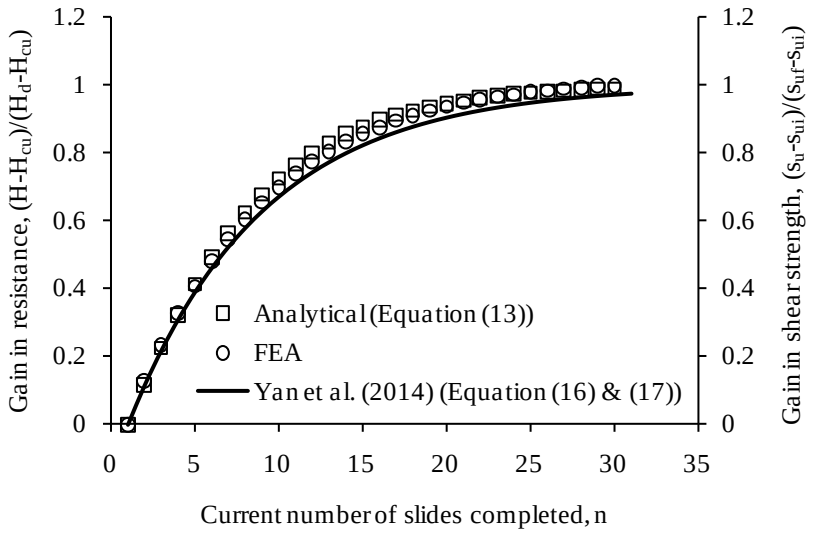

1

2 b) Comparison of simple models and numerical results

3 Figure 10 Analytical model and power law to predict gain in horizontal resistance

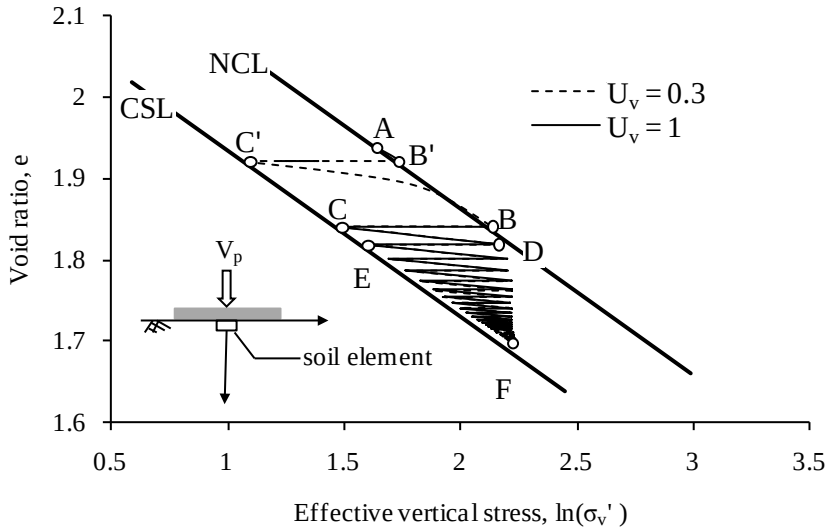

4

5 Figure 11 Comparison of stress-volume path for a soil element for different U_v

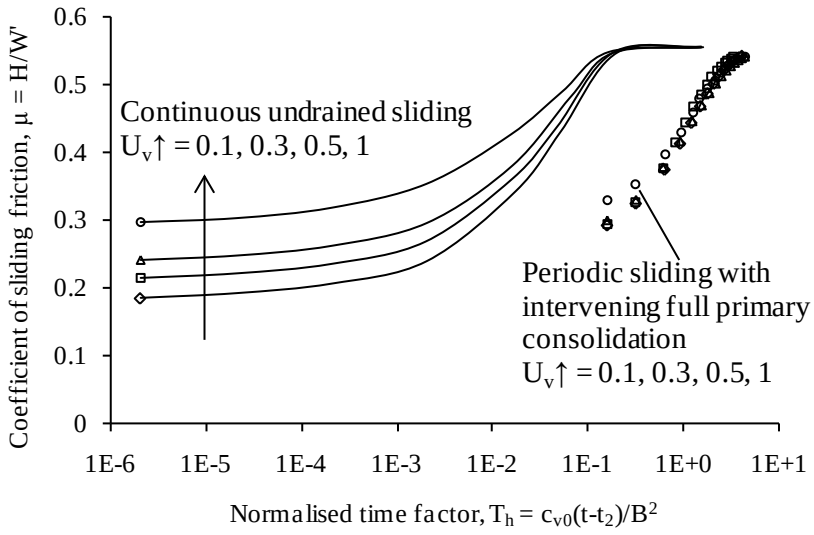

1

2 Figure 12 Hardening process of sliding resistance for periodic shearing

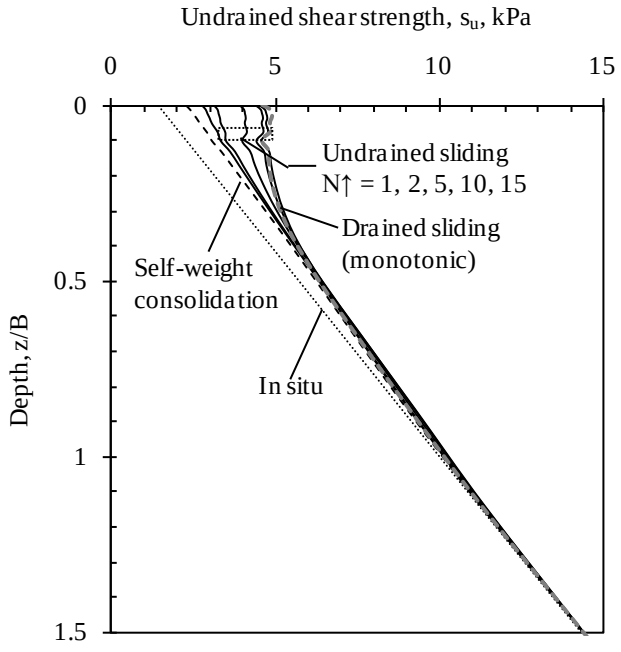

3

4 Figure 13 Profile of soil undrained shear strength during the episodic foundation sliding (U_v

5 =1; U_i =1)

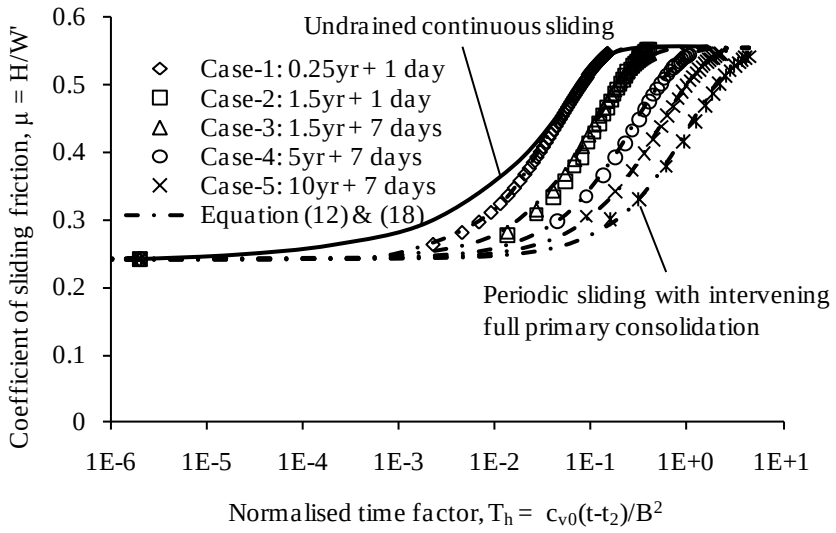

1

2 Figure 14 Responses of a mobile mudmat under periodic shearing with partial intervening

3 consolidation (U_v = 0.5)

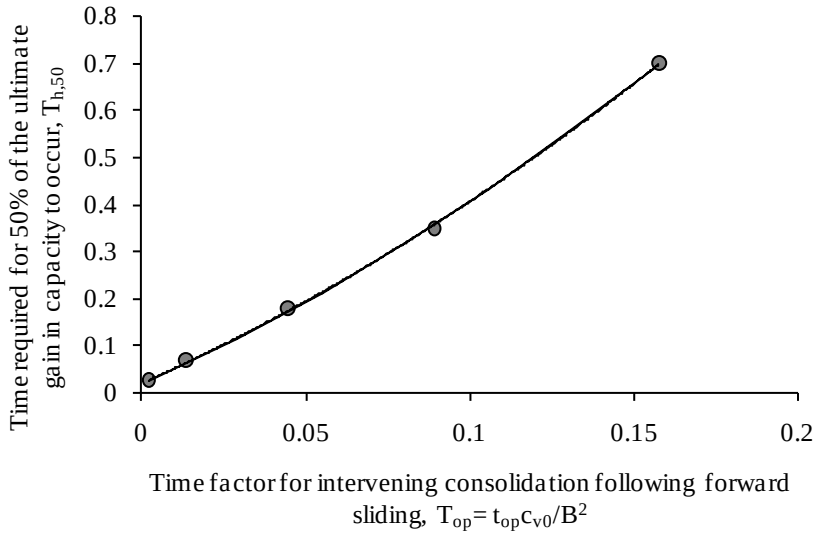

4

5 Figure 15 Evolution of $T_{h,50}$ with varying T_{op}

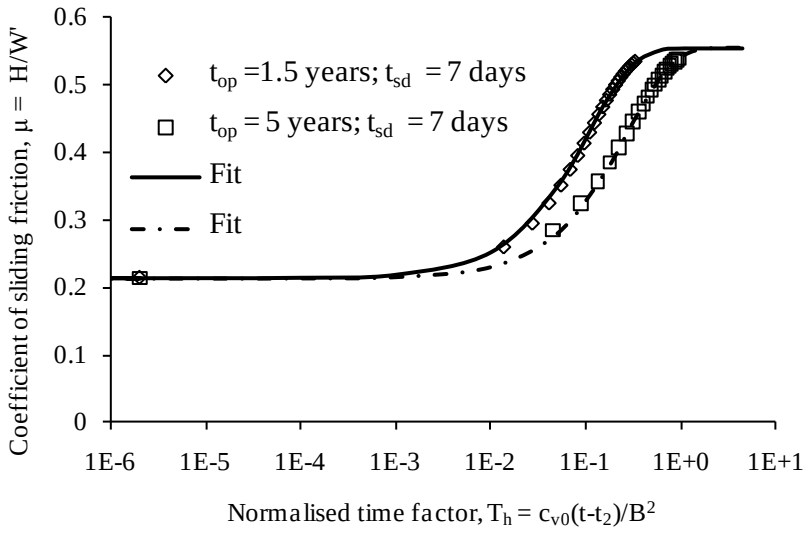

1

2 a) v_p = 0.3, U_v = 0.3, σ_{vo} = 5 kPa

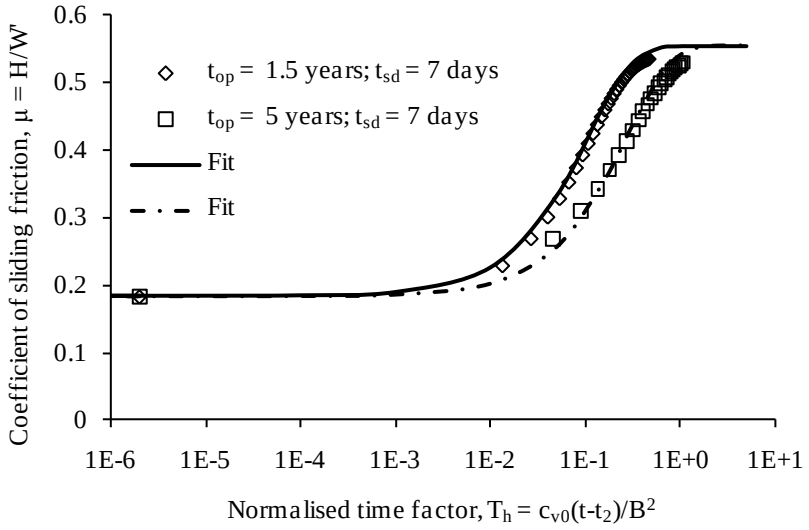

3

4 b) v_p = 0.5, U_v = 0.3, σ_{vo} = 5 kPa

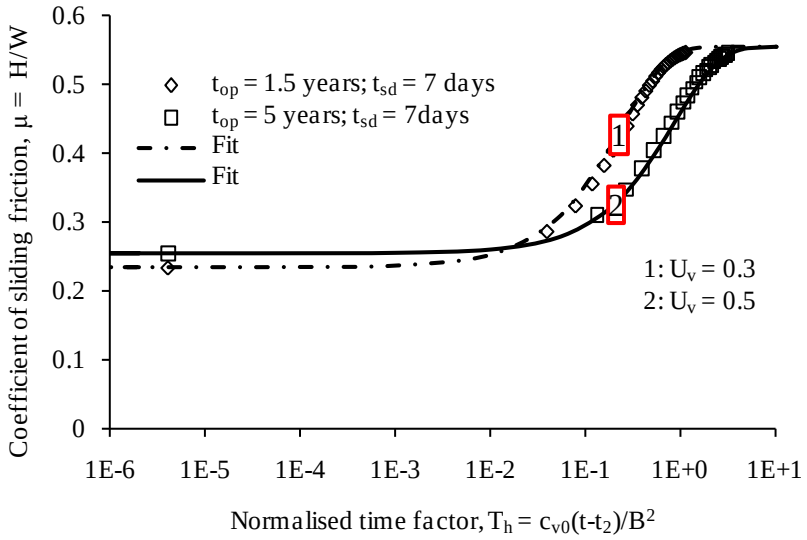

1

2 c) v_p = 0.3, σ_{vo} = 16 kPa

3 Figure 16 Effect of self-weight load, degree of primary consolidation and overburden stress

4 on the hardening process